ACS APPLIED MATERIALS & INTERFACES

Research Article

www.acsami.org

Copper Indium Gallium Selenide (CIGS) Photovoltaic Devices Made Using Multistep Selenization of Nanocrystal Films

Taylor B. Harvey,[†,‡] Isao Mori,[⊥] C. Jackson Stolle,[†,‡] Timothy D. Bogart,[†,‡] David P. Ostrowski,[‡,§] Micah S. Glaz,[‡,§] Jiang Du,[†,‡] Douglas R. Pernik,[†,‡] Vahid A. Akhavan,[†,‡] Hady Kesrouani,[†,‡] David A. Vanden Bout,[‡,§] and Brian A. Korgel[†,‡,*]

[†]Department of Chemical Engineering, [‡]Texas Materials Institute and Center for Nano- and Molecular Science and Technology, and [§]Department of Chemistry, The University of Texas at Austin, Austin, Texas 78712, United States

[⊥]Department of Electronic Engineering, University of Tokyo, Tokyo, Japan

Supporting Information

ABSTRACT: The power conversion efficiency of photovoltaic devices made with ink-deposited $Cu(In_xGa_{1-x})Se_2$ (CIGS) nanocrystal layers can be enhanced by sintering the nanocrystals with a high temperature selenization process. This process, however, can be challenging to control. Here, we report that ink deposition followed by annealing under inert gas and then selenization can provide better control over CIGS nanocrystal sintering and yield generally improved device efficiency. Annealing under argon at 525 °C removes organic ligands and diffuses sodium from the underlying soda lime glass into the Mo back contact to improve the rate and quality of nanocrystal sintering during selenization at 500 °C. Shorter selenization time alleviates excessive $MoSe_2$ formation at the Mo back contact that leads to film delamination, which in turn enables multiple cycles of nanocrystal deposition and selenization to create thicker, more uniform absorber films. Devices with power conversion efficiency greater than 7% are fabricated using the multiple step nanocrystal deposition and sintering process.

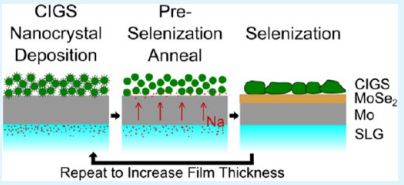

KEYWORDS: *photovoltaics, nanocrystals, selenization, CIGS, copper indium gallium selenide, sodium*

INTRODUCTION

$Cu(In_xGa_{1-x})Se_2$ (CIGS) has strong optical absorption and a favorable band gap for thin film photovoltaics, with the highest reported polycrystalline thin film efficiency of any material of just over 20%.[1] High efficiency devices can be made by coevaporation[2−4] or high temperature annealing of vacuum-sputtered metals under selenium vapor (i.e., selenization).[5] Commercialization of CIGS PVs using these processes has been challenging due to high process complexity,[5−7] relatively large capital requirements,[8] inefficient materials usage,[9,10] and spatial composition and thickness nonuniformity in large-area devices.[6,11,12] Nonvacuum, solvent-based CIGS layer deposition provides an alternative strategy with potentially higher throughput at significantly lower cost.[13]

PV devices with power conversion efficiency (PCE) of just over 3% have been made by room-temperature, ambient spray deposition of $CuInSe_2$ nanocrystals.[14] The electrically insulating organic capping ligands used to stabilize and disperse the nanocrystals in solvents are largely responsible for the limited device efficiency.[15] Replacing the capping ligands with small molecules like metal chalcogenide complexes (MCCs) has improved charge extraction and led to slightly higher device internal quantum efficiency but not yet significant enhancements in PCE.[16] Significantly higher PCE has been achieved by sintering nanocrystals into polycrystalline films.[17,18] For instance, the highest reported efficiency of 12.0% for a solvent-deposited nanocrystal device has been achieved by selenizing a $Cu(In_xGa_{1-x})S_2$ nanocrystal layer.[18,19] Solvent-deposited submicrometer diameter metal oxide particles[20,21] and metal nitrate salt solutions[22] have also been selenized to fabricate CIGS devices with reasonable efficiencies, but composition has been difficult to control over larger areas using these approaches, often with significant oxygen, chloride and nitrate contamination. Selenization of single-phase chalcopyrite $Cu(In_xGa_{1-x})Se_2$ nanocrystals should provide more precise control over layer composition. Significant carbon in these nanocrystal films from the capping ligands, however, has limited device efficiency. The highest reported PCE for selenized $Cu(In_xGa_{1-x})Se_2$ nanocrystals is 5.1%, limited in large part by the formation of a carbon-containing impurity layer.[23] Similar impurity layers have been observed in selenized films of ink-deposited nitrate-containing salts,[22] $CuIn_xGa_{1-x}S_2$ nanocrystals,[17] multiphase $CuInSe_2$ nanoparticles,[24] and $Cu_{2-x}S$ nanoparticle/In acetate mixtures.[25]

Various strategies exist for reducing carbon contamination in solution-processed CIGS films. For instance, the highest device efficiency of a solution-processed CIGS PV of 15.2% was achieved by selenizing carbon-free hydrazine-derived molecular reactants.[26−28] This approach, however, requires highly toxic and potentially explosive hydrazine and would be very costly to

Received: June 27, 2013
Accepted: August 19, 2013
Published: August 19, 2013

use in a manufacturing setting. Nitrate-derived metal salt solutions have been annealed to remove carbon before sulfurization and selenization,[29] but without significant improvement in device efficiency.[22] "Carbon-free" $CuInSe_2$ films have been made by selenizing $Cu_{11}In_9$ nanocrystals capped with disodium citrate, but the formation of significant copper selenide during the process required toxic cyanide (KCN) etching to make functioning PVs.[30] Mixtures of Cu Oxide, In hydroxide, and Ga acetylacetonate dissolved in butyldithiocarbamic acid[31] and aqueous dispersions of CuS and In_2S_3 nanocrystals mixed with Cu and In chlorides[32] have also been selenized to yield devices that are largely carbon-free with 8.8% and 6% efficiency, respectively.

Here, we report that the typical carbon contamination layer in selenized CIGS nanocrystal films can be alleviated by employing a brief heating of a $Cu(In_xGa_{1-x})Se_2$ nanocrystal layer in Ar at 525 °C prior to selenization. This process also drives sodium into the Mo back contact from the underlying soda-lime glass substrate that significantly enhances sintering of the CIGS nanocrystals during selenization and provides better processing control. Shortened selenization time helps retain device integrity by limiting conversion of the Mo back contact to $MoSe_2$. Some $MoSe_2$ is needed because it improves electrical contact with the CIGS layer, but excessive $MoSe_2$ formation leads to film delamination. With increased selenization rates, multiple processing steps of nanocrystal deposition and selenization were employed to create selenized CIGS films that were thicker and more uniform than possible with a single nanocrystal deposition and selenization step. By adding a NaCl salt bath treatment after the initial preselenization anneal, devices with over 7% efficiency could be fabricated from selenized (sulfur-free) $Cu(In_xGa_{1-x})Se_2$ nanocrystals. Light beam-induced current (LBIC) mapping showed that the active regions of devices have significantly enhanced photocurrent when the preselenization anneal is employed.

EXPERIMENTAL DETAILS

Materials. Se powder (99.99%), CuCl (99.99+%), $GaCl_3$ (99.999+%), and $CdSO_4$ (99.999%) was received from Aldrich Chemical Co.; $InCl_3$ (99.999%) from Strem Chemicals; Oleylamine (OLA) from TCI America; Ethanol (absolute), toluene (99.99%), and ammonium hydroxide (18 M NH_3; ACS certified) from Fisher Scientific; and thiourea (>99.0%) from Sigma-Aldrich. Oleylamine was degassed overnight at 110 °C under vacuum. All other chemicals were used without additional purification.

$CuIn_xGa_{1-x}Se_2$ (CIGS) Nanocrystal Synthesis. Published procedures[13,23] were used to synthesize CIGS nanocrystals with a targeted composition of $Cu_{0.8}In_{0.7}Ga_{0.3}Se_2$. In a N_2-filled glovebox, 50 mL of degassed OLA, 5 mmol of CuCl, 2.5 mmol of $InCl_3$, 2.5 mmol of $GaCl_3$, and 10 mmol of Se were added to a three-neck flask. After degassing the mixture at 110 °C for 30 min on a Schlenk line, the flask was filled with nitrogen and the temperature elevated to 200 °C for 30 min, followed by further heating to 260 °C for 10 min. After cooling to room temperature, centrifugation was used to wash the particles using ethanol and toluene as antisolvent and solvent. Toluene was added to the reach a final nanocrystal concentration of 20 mg/mL.

PV Device Fabrication. Sodalime glass (Delta Techology) was sonicated in an acetone/isoproponol mixture, then in DI water, and dried with nitrogen. One micrometer thick Mo (Lesker 99.95%) layers were sputter-coated in two steps; a 400 nm adhesive layer of Mo at 5 mtorr followed by a 600 nm of highly conductive Mo at 1.5 mtorr to give a total sheet resistance of ∼1.0 Ω/□.

CIGS nanocrystals were spray-deposited using an Iwata Eclipse HP-CS spray gun operated at 25 psig head pressure. Films (400−1500 nm thick) were annealed under Ar at temperatures between 425 and 525 °C. Selenization was carried out by placing the substrates into a hollow graphite cylinder in a nitrogen-filled glovebox with a boat of elemental selenium. The chamber was tightly capped and removed from the glovebox and annealed for 10 min at 500 °C.

Following selenization, 50 nm of CdS was deposited by chemical bath deposition (CBD). In a crystallization dish, 160 mL of 18.2 MΩ DI water was heated to 80 °C. Twenty-five milliliters of 15 mM $CdSO_4$, 12.5 mL of 1.5 M thiourea, and 32 mL of ammonium hydroxide were added and the selenized films were immersed for 15 min. Fifty nanometers of ZnO (99.9% Lesker) was sputtered in a 5 ppm O_2/Ar atmosphere, followed by sputtering of a 600 nm ITO (99.99% Lesker) layer in an Ar atmosphere through physical shadow masks to create a 10 mm by 2.5 mm active area. Silver paint grids were added to increase lateral conductivity, reducing the active area to 10 mm^2. Performance was improved by baking completed devices up to 24 h at 200 °C.

Materials and Device Characterization. Current−potential (IV) characteristics were collected using a Keithley 2400 source meter under AM1.5G illumination (100 mW/cm^2). A NIST calibrated Si photodiode (Hamamatsu, S1787−08) was used to tune light intensity. External quantum efficiency (EQE) was measured as previously described.[14,23] Monochromatic light (Newport Cornerstone 260 1/4M) at wavelengths ranging from 300 to 1300 nm in 10 nm steps was chopped at 213 Hz and focused to a 1 mm diameter spot size on the device at zero bias. EQE was measured using a lock-in-amplifier (Stanford Research Systems, model SR830) after calibrating light intensity with silicon (Hamamatsu) and germanium (Judson) photodiodes.

Scanning electron microscope (SEM) images were collected after CdS deposition with the InLens detector of a Zeiss microscope operating at 5 kV. Thermogravimetric analysis (TGA) was collected using a Mettler-Toledo DCS/TGA instrument with a temperature ramp of 20 °C/min followed by a temperature hold at 425, 475, or 525 °C for 1 h. Nanocrystal composition was verified via energy-dispersive X-ray spectroscopy (EDS) carried out on a Quanta 650 FEG SEM equipped with a Bruker XFlash EDS Detector 5010. EDS spectra of nanocrystals drop-cast on a Si wafer were generated at 20 kV accelerating voltage and a working distance of 10 mm with a spot size of 5. EDS spectra were integrated to determine nanocrystal composition with Bruker ESPRIT software.

XPS data were taken using a Kratos (Axis Ultra) instrument, utilizing a monochromated 1486.5 eV Al−K_α X-ray source. Spectra were collected using a pass energy of 20 at 0.1 eV intervals and 1500 ms integration time with a 300 μm × 700 μm aperture. A Shirley baseline was used for background subtraction and sample charging was corrected by shifting the Mo^0 $3d_{5/2}$ to a binding energy of 228.0 eV. The Mo 3d region was fit using Voigt profiles (30% Gaussian character) with peak centers at 228.0, 228.7, 232.2, and 232.8 eV corresponding to Mo^0, $MoSe_2$, Na_xMoO_y, and MoO_3, respectively, for the $3d_{5/2}$ spin. The $3d_{3/2}$ peaks were centered at +3.13 eV from their $3d_{5/2}$ counterparts with the intensity ratio held at 3:2 in congruence with the spin−orbit splitting for Mo d-orbitals. Casa XPS was used with Kratos sensitivity factors to determine the elemental composition of the samples.

Light beam-induced current (LBIC) microscopy was collected in the same manner as previously described.[23,35] Image maps were created by scanning a 473 nm laser (CrystaLaser) at a power of 38 ± 4 nW over devices and measuring the photocurrent at each step.

RESULTS AND DISCUSSION

PV devices were fabricated by spray-depositing a 800 nm layer of oleylamine-capped $Cu_{0.8}(In_{0.7}Ga_{0.3})Se_2$ nanocrystals approximately 15 nm in diameter on Mo-coated soda-lime glass followed by selenization in a tightly capped graphite cylinder. We have shown previously that sintering the CIGS nanocrystals in this closed chamber traps carbon eliminated from the nanocrystal film and leads to a residual coating carbon and selenium, which LBIC maps revealed to diminish device performance.[23] This motivated us to explore a preselenization

anneal to remove most of the organic ligand from the nanocrystal film prior to being placed in the selenization chamber. TGA of CIGS nanocrystals (Figure 1a) showed that

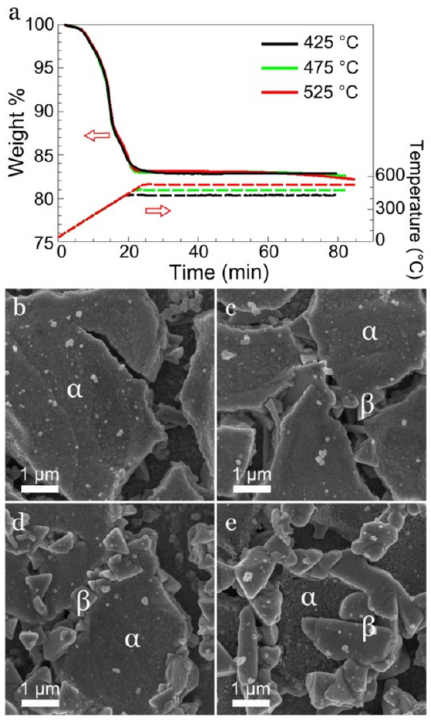

Figure 1. (a) Residual mass determined by TGA and the corresponding sample temperature profile. Samples were heated under nitrogen to final temperatures of 425, 475, or 525 °C. The TGA analysis was carried out under conditions similar to those used in the preselenization anneal. (b–e) SEM of the selenized nanocrystal layers (b) without a preselenization anneal and with preselenization anneals at (c) 425, (d) 475, and (e) 525 °C under Ar for 1 h. The labels α and β indicate unsintered and sintered regions of the film, respectively.

complete removal of organics occurs at about 425 °C. Still, there was a noticeable difference in the quality of the selenized films depending on the preanneal temperature. Figure 1 shows SEM images of selenized nanocrystal films that were annealed at 425 °C, 475 and 525 °C prior to selenization at 500 °C. The nanocrystal films heated to the highest preselenization temperature of 525 °C exhibited the most sintering and crystal grain growth during selenization (the sintered domains have a triangular morphology).

Table 1 shows the performance of selenized CIGS nanocrystal PV devices—the preselenization temperature was found to significantly affect the device PCE. Films without a preselenization anneal did not exhibit any measurable short circuit current, whereas the preselenization at 525 °C led to devices with efficiency as high as 4.17%. The very poor device performance of the layers without the preselenization anneal resulted in part from the very short selenization time of only 10 min. For comparison, recently reported selenized $Cu_{0.82}In_{0.32}Ga_{0.68}Se_2$ nanocrystal devices with 5.1% efficiency were selenized for 1 h at 500 °C.[23]

Table 1. Performance of PV Devices Fabricated Using Different Preselenization Anneal Temperatures (1 h heating under Ar) Followed by a 10 min Selenization at 500°C[a]

preselenization anneal temp (°C)	V_{oc} (V)	J_{sc} (mA/cm^2)	FF	PCE (%)
no anneal	0.00	0.00	0.00	0.00
425	0.14	3.33	0.27	0.08
475	0.36	7.19	0.33	0.82
525	0.53	17.88	0.44	4.17

[a]Measurements were made with 100 mW/cm^2 AM1.5 illumination.

Because TGA showed that the organic weight loss is similar for all three preselenization annealing temperatures in Table 1, the difference in device efficiency is not due to ligand removal. XPS (Figure 2) analysis of the Mo back contact after Mo-coated soda lime glass substrates were heated under Ar for 1 h showed a considerable Na signal, which increased with increasing annealing temperature. Sodium is known to enhance CIGS crystal grain growth during selenization.[18,33,34] The most important contribution of the preselenization anneal to achieving more effective selenization of CIGS nanocrystal films appears to be sodium addition from the underlying substrate. XPS of the nanocrystal layers on Mo after preselenization anneal, however, did not show any Na even after 5 min of Ar sputtering, implying that Na does not diffuse into the nanocrystal layer to a significant extent during the preselenization anneal (see Figure S1 in the Supporting Information). These data suggest that Na diffuses from the soda-lime glass to the Mo/CIS interface during the preselenization anneal. Figure 3 shows LBIC maps of PV devices made from selenized CIGS nanocrystal films with preselenization anneals at 525 and 475 °C. There is significant

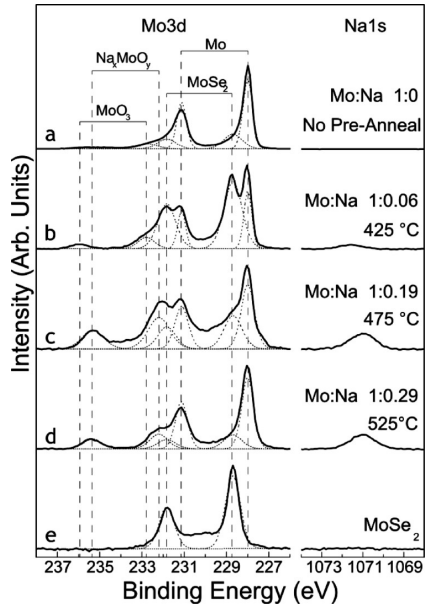

Figure 2. XPS data: Mo 3d and Na 1s regions measured from molybdenum-coated soda-lime glass (a) before and (b–e) after annealing under Ar for 1 h at (b) 425 °C, (c) 475 °C, (d) 525 °C, and (e) selenized at 525 °C for 10 min. The Mo 3d region was fit by adding separate peak contributions from Mo^0, $MoSe_2$, MoO_3, and Na_xMoO_y for both $3d_{5/2}$ and $3d_{3/2}$ spin. Na 1s signal was normalized to the maximum intensity of the corresponding Mo 3d signal. The total integrated Mo 3d peak was used to normalize the Mo:Na response from sample to sample. $MoSe_2$ formation occurs from residual Se in the tube furnace. Additionally, some MoO_3 and Na_xMoO_y was detected because of oxidation of the Mo back contact.

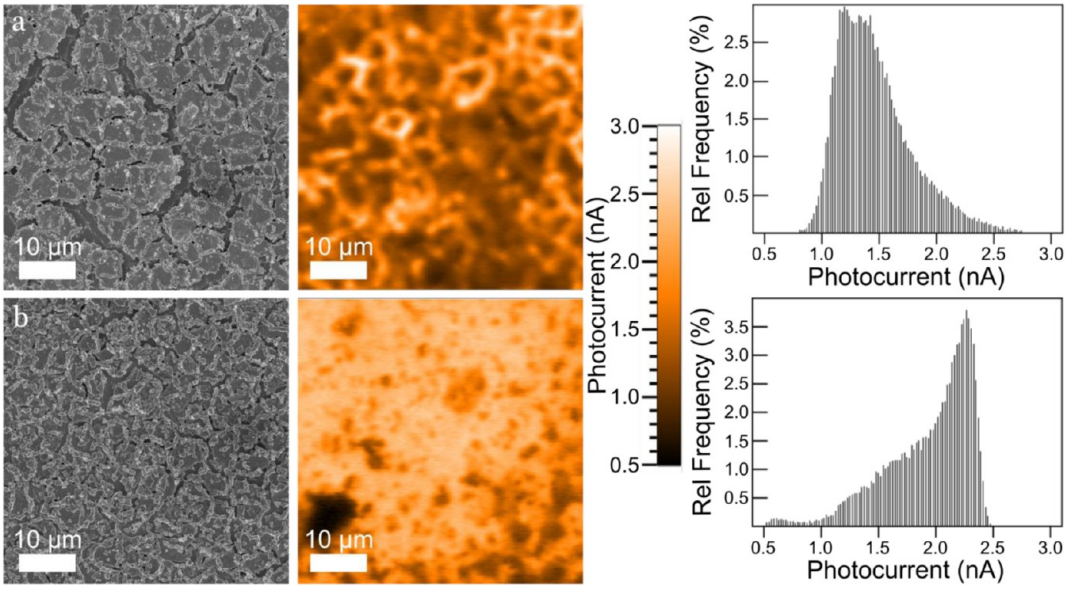

Figure 3. SEM image (left), LBIC map (middle), and photocurrent histogram (right) of PV devices made with selenized CIGS nanocrystals with a preselenization anneal under Ar for 1 h at (row a) 475 and (row b) 525 °C. The CIGS layer with preselenization anneal at 525 °C shows higher photocurrent.

inhomogeneity in both device layers, but the photoresponse of the active regions in the CIGS layer with the 525 °C preselenization anneal is significantly higher than in the CIGS layer with the 475 °C preselenization anneal, consistent with the much higher short circuit current and device efficiency (Table 1).

The absence of sodium diffusion into the nanocrystal film during the preselenization anneal results in enhanced sintering of the nanocrystals only near the Mo back contact. Figure 4 shows SEM images of cross-sectioned selenized CIGS layers of varying thickness. The relatively thin CIGS nanocrystal layer (400 nm) does sinter uniformly throughout the entire film. However, the thicker 1.6 μm film sinters near the Mo substrate and toward the top of the film exposed to Se. There is a relatively thick inner region of nanocrystals that remain unsintered. Se does not seem to be able to penetrate deep into the nanocrystal film to promote sintering effectively, although nanocrystal sintering is observed near the substrate where the Na concentration would be highest. This is important because the 400 nm films are too thin to absorb a significant portion of the incident light. The highest efficiency devices made by coevaporation have CIGS layers around 2 μm thick.[2] Strategies for uniform sintering of thicker CIGS nanocrystal layers are needed.

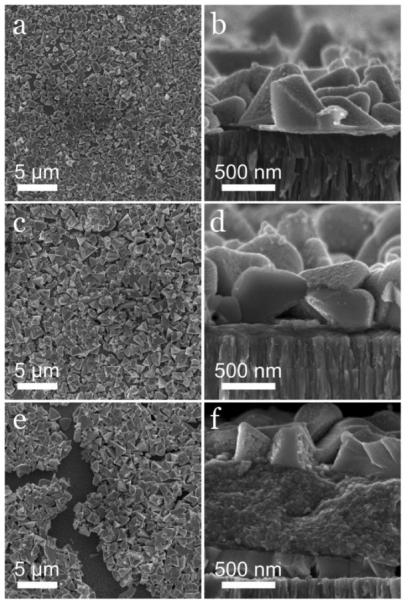

Figure 4. Top-view and cross-section SEM images of CIGS nanocrystal films selenized on Mo-coated soda lime glass substrates with different thickness: (a, b) 0.4 μm, (c, d) 0.8 μm, (e, f) 1.6 μm. All films were heated under Ar for 1 h at 525 °C prior to selenization for 10 min at 500 °C.

One approach to sodium infusion into the CIGS nanocrystal film is to soak the layer in a NaCl bath as first reported by Guo, et al.[18] in their work to significantly improve device performance from selenized $Cu(In_xGa_{1-x})S_2$ nanocrystal films. We have found that a NaCl bath can also improve CIGS nanocrystal selenization. Figure 5 shows SEM and LBIC images of two CIGS nanocrystal films annealed at 475 °C under Ar for 1 h and then selenized at 500 °C for 10 min. The nanocrystal device layer in Figure 5b was also soaked in aqueous 1 M NaCl for 10 min prior to selenization. The film with the NaCl bath treatment exhibited significantly higher photocurrent in the active device regions. The NaCl-soaked films also had some inactive regions that appear to result from residual NaCl.

We have found that limiting the selenization time is important for maintaining the integrity of the device. The Mo bottom contact reacts with Se to form $MoSe_2$ and some conversion of Mo to $MoSe_2$ is important to improve electrical contact with the CIGS film, but excess $MoSe_2$ formation leads to delamination of the CIGS layer. Mo selenization occurs at temperatures as low as 350 °C.[36] Figure 6 shows SEM images of cross-sectioned CIGS layers on Mo-coated glass substrates selenized for 10 min at 500 °C with a 525 °C preselenization anneal under Ar with three different heating rates. The extent of $MoSe_2$ formation is limited by minimizing the time in the 350–500 °C temperature range—the thickness of the $MoSe_2$ layer

dx.doi.org/10.1021/am4025142 | ACS Appl. Mater. Interfaces 2013, 5, 9134–9140

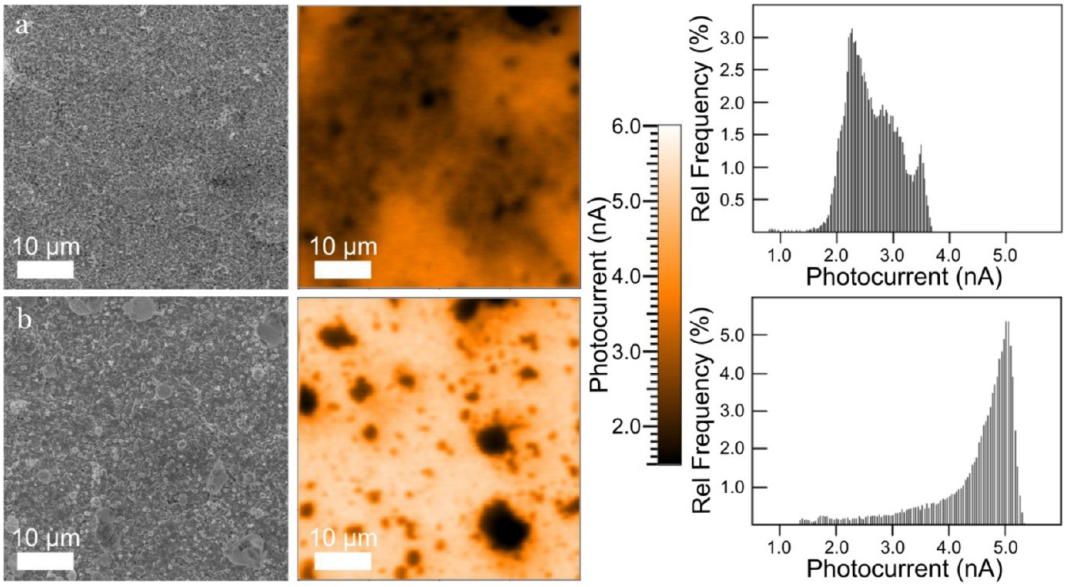

Figure 5. SEM image (left), LBIC map (middle), and photocurrent histogram (right) of devices (row a) without and (row b) with soaking for 10 min in aqueous 1 M NaCl. The nanocrystal films in a and b were annealed under Ar for 1 h at 475 °C prior to NaCl bath soaking and selenization for 10 min at 500 °C.

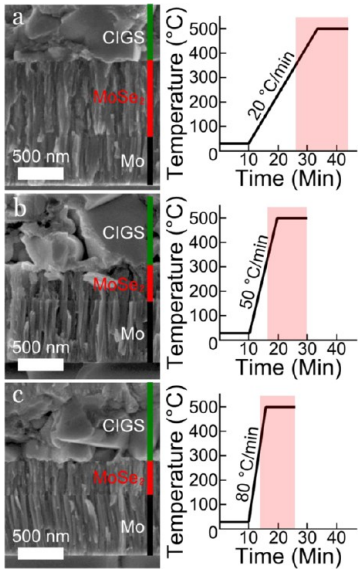

Figure 6. SEM images of cross-sectioned CIGS nanocrystal films on Mo-coated soda lime glass substrates after selenization at 500 °C for 10 min with temperature ramping of (a) 20, (b) 50, and (c) 80 °C/min. The temperature profile is shown on the right of each image. The temperature range between 350 and 500 °C is highlighted in pink.

was decreased by a factor of 2 when the heating ramp rate was increased from 20 °C/min (Figure 6a) to 50 °C/min (Figure 6b). Increasing the ramp rate further to 80 °C/min, however, (Figure 6C) did not change the $MoSe_2$ thickness, consistent with the fact that the time spent in the 350−500 °C temperature range (12 min vs 13 min) was not significantly different.

As shown in Figure 4, CIGS nanocrystal films greater than about 800 nm thick do not completely sinter through the entire film. Unsintered portions in the film lead to poor device performance. For complete light absorption and the highest possible device efficiency, thicker selenized CIGS layers are needed. A further problem with devices made with only a single nanocrystal deposition and selenization step is that the selenized layer does not uniformly cover the substrate due to the formation of voids during the crystallization of the nanocrystal film. An additional step of nanocrystal deposition can fill the voids in the film and build thicker layers, but the total selenization time must be limited because the film delaminates if too much $MoSe_2$ forms at the back contact. The use of a 525 °C preselenization anneal, NaCl bath soak, and fast ramp rate to the selenization temperature allows the selenization time to be limited to 10 min and PVs can then be made with selenized CIGS nanocrystal films of up to 2 μm thick by repeating the deposition, preselenization anneal, and selenization process (as shown in Figure 7).

Figure 8 compares SEM images of selenized CIGS nanocrystal layers made with one, two or three cycles of nanocrystal deposition and selenization. The spatial coverage of the substrate becomes more uniform with multiple cycles of deposition and selenization. The average sintered grain size also

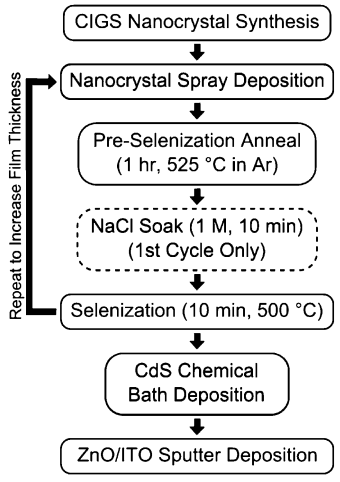

Figure 7. Process steps used to fabricate CIGS PVs with 2 μm CIGS absorber layers.

dx.doi.org/10.1021/am4025142 | ACS Appl. Mater. Interfaces 2013, 5, 9134−9140

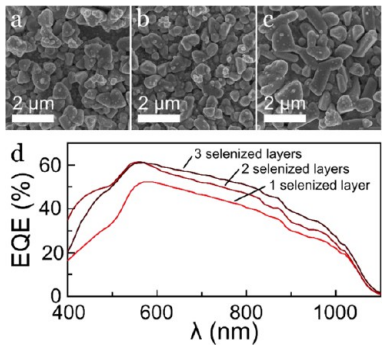

Figure 8. SEM images of selenized CIGS nanocrystal layers made with (a) one, (b) two, or (c) three cycles of CIGS nanocrystal deposition, 525 °C preselenization anneal in Ar for 1 h, and a 10 min selenization at 500 °C. (d) EQE for devices made with the indicated number of deposition/selenization steps.

increases with more deposition/selenization steps. Figure 9 shows device characteristics and SEM images of one of the best

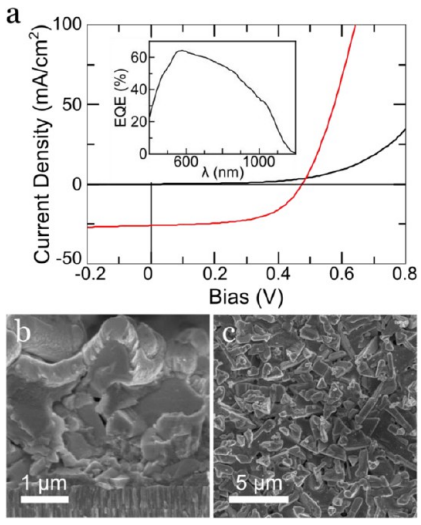

Figure 9. (a) PV device response for a selenized CIGS nanocrystal device with 7.1% power conversion efficiency under AM1.5 illumination (100 mW/cm^2). The device was made using three sequential nanocrystal deposition/selenization steps. The EQE is shown in the inset. (b) SEM image of a device cross-section showing that the sintered CIGS layer is more than 2 μm thick. (c) SEM of the CIGS layer from the top, showing relatively large sintered CIGS crystal grains.

devices made using multiple deposition/sintering cycles. This device was made with 3 deposition/selenization cycles and had a sintered CIGS film thickness of about 2 μm with a PCE of 7.1%. Table 2 summarizes the performance of devices made with one, two, or three repetitions of the deposition, preselenization anneal, selenization. A steady rise in PCE is observed as the film thickness was increased, mostly due to higher V_{oc} and FF; however, a small rise in J_{sc} is also seen. In Figure 8d, the maximum EQE rose when the device was made with two deposition/selenization cycles instead of one. The device EQE primarily increased at longer wavelengths when three cycles were used instead of two, indicating more light absorption from the thicker film but probably slightly decreased IQE. A decrease in the number of grain boundaries (Figure 9b)

Table 2. Performance of PV Devices Made Using Various Cycles of CIGS Nanocrystal Deposition, 525 °C Preselenization Anneal under Ar for 1 h, and 10 min Selenization at 500 °C with a 10 min Soak in Aqueous 1 M NaCl after the First Preselenization Anneal[a]

no. of deposition/selenization cycles	V_{oc} (V)	J_{sc} (mA/cm^2)	FF	PCE (%)
1	0.43	20.5	0.37	3.26
2	0.47	21.8	0.42	4.32
3	0.51	22.1	0.49	5.01
3 (optimized)	0.48	25.9	0.58	7.1

[a]The "optimized" device was made by depositing thicker nanocrystal layers (~1 μm) during each cycle.

and improved film uniformity are expected to improve device performance further.

CONCLUSIONS

PV devices were fabricated with selenized Cu(In_xGa_{1-x})Se_2 nanocrystal films to achieve power conversion efficiency of up to 7.1%. These devices were made by three cycles of spray-deposition of CIGS nanocrystals followed by selenization. Multiple nanocrystal/selenization steps were enabled by the use of a high temperature preselenization anneal under inert atmosphere for 1 h to remove capping ligands and drive sodium from the glass substrate to the Mo/nanocrystal interface prior to selenization at 500 °C. This preselenization anneal made nanocrystal sintering during selenization occur much more rapidly and a relatively short 10 min selenization time was needed to sinter the nanocrystals compared to a typical selenization time of 1 h. The use of a NaCl bath soak of the nanocrystal films was also found to help improve sintering uniformity in thicker nanocrystal layers.

ASSOCIATED CONTENT

Supporting Information

XPS measurements of a CIGS film after 525 °C preselenization anneal. Spectra were collected before and after Ar+ sputtering. This material is available free of charge via the Internet at http://pubs.acs.org.

AUTHOR INFORMATION

Corresponding Author

*E-mail: korgel@che.utexas.edu. Phone: +1-512-471-5633. Fax: +1-512-471-7060.

Notes

The authors declare no competing financial interest.

ACKNOWLEDGMENTS

Financial support of this work was provided by the Robert A. Welch Foundation (F-1464) and the National Science Foundation Industry/University Cooperative Research Center on Next Generation Photovoltaics (IIP-1134849). I.M. acknowledges support by the "Nanotechnology Platform" of the Ministry of Education, Culture, Sports, Science and Technology(MEXT), Japan. C.J.S. acknowledges support from the National Science Foundation Graduate Research Fellowship under Grant DGE-1110007. T.D.B. acknowledges support from the Department of Defense (DoD) through the National Defense Science & Engineering Graduate Fellowship (NDSEG) Program. H.K. performed this research as part of a

student exchange agreement between The University of Texas at Austin and the Ecole Centrale de Lille, France.

REFERENCES

(1) Jackson, P.; Hariskos, D.; Lotter, E.; Paetel, S.; Wuerz, R.; Menner, R.; Wischmann, W.; Powalla, M. *Prog. Photovoltaics Res. Appl.* **2011**, *19*, 894−897.
(2) Repins, I.; Contreras, M. A.; Egaas, B.; DeHart, C.; Scharf, J.; Perkins, C. L.; To, B.; Noufi, R. *Prog. Photovoltaics Res. Appl.* **2008**, *16*, 235−239.
(3) Kessler, J.; Wennerberg, J.; Bodegård, M.; Stolt, L. *Sol. Energy Mater. Sol. Cells* **2003**, *75*, 35−46.
(4) Wallin, E.; Malm, U.; Jarmar, T.; Edoff, Olle Lundberg, M.; Stolt, L. *Prog. Photovoltaics Res. Appl.* **2012**, *20*, 851−854.
(5) Goushi, Y.; Hakuma, H.; Tabuchi, K.; Kijima, S.; Kushiya, K. *Sol. Energy Mater. Sol. Cells* **2009**, *93*, 1318−1320.
(6) Voorwinden, G.; Kniese, R.; Powalla, M. *Thin Solid Films* **2003**, *431−432*, 538−542.
(7) Powalla, M.; Voorwinden, G.; Hariskos, D.; Jackson, P.; Kniese, R. *Thin Solid Films* **2009**, *517*, 2111−2114.
(8) Zweibel, K. *Sol. Energy Mater. Sol. Cells* **1999**, *59*, 1−18.
(9) Liehr, M. In *Proceedings of the 3rd International Workshop Thin Films in the Photovoltaic Industry*; Ispra, Italy, Nov 22−23, 2007 ; Office for Official Publications of the European Communities: Luxembourg, **2007**,.
(10) Wilkommen, U.; Diemer, M. In *Proceedings of the 3rd International Workshop Thin Films in the Photovoltaic Industry*; Ispra, Italy, Nov 22−23, 2007 ; Office for Official Publications of the European Communities: Luxembourg, **2007**,.
(11) Bauer, G. H.; Gütay, L.; Kniese, R. *Thin Solid Films* **2005**, *480−481*, 259−263.
(12) Karg, F. *Energy Procedia* **2012**, *15*, 275−282.
(13) Panthani, M. G.; Akhavan, V.; Goodfellow, B.; Schmidtke, J. P.; Dunn, L.; Dodabalapur, A.; Barbara, P. F.; Korgel, B. A. *J. Am. Chem. Soc.* **2008**, *130*, 16770−16777.
(14) Akhavan, V. A.; Panthani, M. G.; Goodfellow, B. W.; Reid, D. K.; Korgel, B. A. *Opt. Express* **2010**, *18*, A411−A420.
(15) Akhavan, V. A.; Goodfellow, B. W.; Panthani, M. G.; Reid, D. K.; Hellebusch, D. J.; Adachi, T.; Korgel, B. A. *Energy Environ. Sci.* **2010**, *3*, 1600.
(16) Stolle, C. J.; Panthani, M. G.; Harvey, T. B.; Akhavan, V. A.; Korgel, B. A. *ACS Appl. Mater. Interfaces* **2012**, *4*, 2757−2761.
(17) Guo, Q.; Ford, G. M.; Hillhouse, H. W.; Agrawal, R. *Nano Lett.* **2009**, *9*, 3060−3065.
(18) Guo, Q.; Ford, G. M.; Agrawal, R.; Hillhouse, H. W. *Prog. Photovoltaics Res. Appl.* **2013**, *21*, 64−71.
(19) Stolle, C. J.; Harvey, T. B.; Korgel, B. A. *Curr. Opin. Chem. Eng.* **2013**, *2*, 160−167.
(20) Eberspacher, C.; Fredric, C.; Pauls; Jack Serra, K. *Thin Solid Films* **2001**, *387*, 18−22.
(21) Kapur, V. K.; Bansal, A.; Le, P.; Asensio, O. I. *Thin Solid Films* **2003**, *431−432*, 53−57.
(22) Kaelin, M.; Rudmann, D.; Kurdesau, F.; Zogg, H.; Meyer, T.; Tiwari, A. N. *Thin Solid Films* **2005**, *480−481*, 486−490.
(23) Akhavan, V. A.; Harvey, T. B.; Stolle, C. J.; Ostrowski, D. P.; Glaz, M. S.; Goodfellow, B. W.; Panthani, M. G.; Reid, D. K.; Vanden Bout, D. A.; Korgel, B. A. *ChemSusChem* **2013**, *6*, 481−486.
(24) Jeong, S.; Lee, B.-S.; Ahn, S.; Yoon, K.; Seo, Y.-H.; Choi, Y.; Ryu, B.-H. *Energy Environ. Sci.* **2012**, *5*, 7539−7542.
(25) Cho, A.; Ahn, S.; Yun, J. H.; Gwak, J.; Song, H.; Yoon, K. *J. Mater. Chem.* **2012**, *22*, 17893−17899.
(26) Todorov, T. K.; Gunawan, O.; Gokmen, T.; Mitzi, D. B. *Prog. Photovoltaics Res. Appl.* **2013**, *21*, 82−87.
(27) Mitzi, D. B.; Yuan, M.; Liu, W.; Kellock, A. J.; Chey, S. J.; Deline, V.; Schrott, A. G. *Adv. Mater.* **2008**, *20*, 3657−3662.
(28) Liu, W.; Mitzi, D. B.; Yuan, M.; Kellock, A. J.; Chey, S. J.; Gunawan, O. *Chem. Mater.* **2010**, *22*, 1010−1014.
(29) Lee, E.; Park, S. J.; Cho, J. W.; Gwak, J.; Oh, M.-K.; Min, B. K. *Sol. Energy Mater. Sol. Cells* **2011**, *95*, 2928−2932.
(30) Kind, C.; Feldmann, C.; Quintilla, A.; Ahlswede, E. *Chem. Mater.* **2011**, *23*, 5269−5274.
(31) Wang, G.; Wang, S.; Cui, Y.; Pan, D. *Chem. Mater.* **2012**, *24*, 3993−3997.
(32) Cai, Y.; Ho, J. C. W.; Batabyal, S. K.; Liu, W.; Sun, Y.; Mhaisalkar, S. G.; Wong, L. H. *ACS Appl. Mater. Interfaces* **2013**, *5*, 1533−1537.
(33) Probst, V.; Karg, F.; Rimmasch, J.; Riedl, W.; Stetter, W.; Harms, H.; Eibl, O. *MRS Online Proc. Libr.* **1996**, *426*, 165−176.
(34) Rau, U.; Schock, H. W. *Appl. Phys. A: Mater. Sci. Process.* **1999**, *69*, 131−147.
(35) Ostrowski, D. P.; Glaz, M. S.; Goodfellow, B. W.; Akhavan, V. A.; Panthani, M. G.; Korgel, B. A.; Vanden Bout, D. A. *Small* **2010**, *6*, 2832−2836.
(36) Koo, J.; Jeon, S.; Oh, M.; Cho, H.; Son, C.; Kim, W. K. *Thin Solid Films* **2013**, *535*, 148−153.